



Reachability analysis on optimal trim state for aerial docking

Ying Liu^a, Jun Wang^a, Quan Quan^{b,*}, Guang-Xun Du^c, Lei Yang^a

^a Air Force Command College, Beijing, 100097, China

^b School of Automation Science and Electrical Engineering, Beihang University, Beijing, 100191, China

^c China Academy of Electronics and Information Technology, Beijing, 100041, China

ARTICLE INFO

Article history:

Received 29 November 2018

Received in revised form 22 November 2020

Accepted 26 December 2020

Available online 13 January 2021

Communicated by Huihe Qiu

Keywords:

Aerial refueling

Docking

Reachability

Trim

Controllability

ABSTRACT

Aerial refueling is an important capability to increase the endurance and flight range of aircraft, but it often suffers from a low success rate. The altitude and speed of the tanker aircraft in the docking phase play a great role in the docking success rate. According to this, the optimal trim state, namely the optimal speed and altitude of the tanker aircraft, is investigated through the reachability analysis method in this paper. The optimal problem is transformed to find the trim state corresponding to the maximum volume of the reachable set. First, a relative motion model of the receiver aircraft with respect to the drogue is proposed. Then, based on reachability analysis, an optimization problem is formulated and a solution procedure is given in detail. In the simulation, the volumes of reachable sets are plotted with respect to the given discrete speeds and altitudes, based on which the optimal trim state of the docking phase is determined. Finally, the determined optimal trim state is verified by using numerous docking control simulations and the degree of controllability from another aspect. The effectiveness of the proposed method is demonstrated.

© 2021 Elsevier Masson SAS. All rights reserved.

1. Introduction

Aerial Refueling (AR) is very important to military missions as it can extend the endurance and flight range of aircraft [1]. During an AR process, the receiver aircraft first breaks away from its formation, then approaches the rear of the tanker aircraft for docking. Once the receiver aircraft completes refueling, the receiver aircraft disconnects with the tanker aircraft and rejoins the formation again. Therefore, the entire process can be decomposed into three phases: the approaching tanker phase, the docking phase, and the rejoin formation phase [2]. This paper will focus on the docking phase which is the key step of an AR process. Currently, AR processes are realized by experienced pilots of manned aircraft or autopilots of Unmanned Aerial Vehicles (UAVs) which often suffer from low success rates.

In fact, inappropriate docking speeds and docking altitudes will affect the docking success rate, but little attention has been paid. The related references about existing chosen docking speeds and

docking altitudes are summarized in Table 1. In [3], a deep learning based trajectory optimization method was provided to decrease the bow wave effect on the drogue, where the refueling altitude was set to be 7010 m and the speed of tanker aircraft was 200 m/s. In [4], a novel docking controller with probe direct control and learning-based preview method was proposed, where the tanker aircraft flew at a velocity of 200 m/s and an altitude of 7010 m. In [5], an adaptive control method was used to reject the trailing vortex, where the altitude was 1524 m and the docking speed was 152 m/s. A mission-oriented flying qualities evaluation approach was proposed to evaluate the closed-loop motion characteristic parameters of the receiver aircraft in [6], where the refueling altitude and the speed of the tanker aircraft were set to be 7600 m and 195 m/s respectively. The receiver forebody aerodynamic effect on the drogue transient motion was considered in [7], where the speed of tanker aircraft was 118 m/s and the docking altitude was 2286 m. Furthermore, a docking control method based on iterative learning control was proposed to compensate the docking errors caused by aerodynamic disturbances in [8], where the docking altitude in this paper was set to be 3000 m and the docking speed was 120 m/s. In [9], a simple method was used to model the receiver forebody aerodynamic effect, where the altitude of the tanker aircraft was 3000 m and the docking speed was 120 m/s. The type of the tanker aircraft is Boeing 707 and the receiver aircraft is F/A-18B. In [10], the dynamic modeling and simulation application of the receiver aircraft are studied, where the altitude of the tanker air-

* Corresponding author.

E-mail address: qq_buaa@buaa.edu.cn (Q. Quan).

Nomenclature

\mathbf{x}_r	state vector of the receiver aircraft	L	lift of the receiver aircraft
\mathbf{x}_t	state vector of the tanker aircraft	D	drag of the receiver aircraft
$\Delta \mathbf{x}$	relative state vector between the tip of the probe and the center of the drogue	ρ	air density
$\Delta \mathbf{x}_r$	relative state vector between the mass center of the receiver aircraft and the center of the drogue	m	mass of the receiver aircraft
T	the force of thrust	\mathcal{D}	target set
		$pre_{\tau}(\mathcal{D})$	reachable set
		$\varphi(h_0, V_0)$	volume of the reachable set at the trim state (h_0, V_0)

Table 1

Summary of the Simulation Experiments and the Actual Flight Test Experiments.

Ref.	The Tanker	The Receiver	Altitude	Docking Speed
[3]	NA	NA	7010 m	200 m/s
[4]	NA	NA	7010 m	200 m/s
[5]	NA	NA	1524	152 m/s
[6]	NA	NA	7600	195 m/s
[7]	NA	NA	2286	118 m/s
[8]	NA	NA	3000 m	120 m/s
[9]	Boeing 707	F/A-18B	3000 m	120 m/s
[10]	NA	NA	7010 m	200 m/s
[11]	F/A-18	F/A-18	2286, 3200, 7620, 9144 m	90 ~ 152 m/s
[12]	Boeing 707-300	F/A-18	NA	NA
[13]	VC-10, KC-10	F-16A	1524 ~ 6096 m	118 ~ 165 m/s

craft was 7010 m and the docking speed was 200 m/s. In [11], the actual flight test experiment was performed by NASA. The type of the tanker aircraft and the receiver aircraft is F/A-18. The docking altitudes were 2286 m, 3200 m, 7620 m, 9144 m and the range of the docking speed was from 90 m/s to 152 m/s. In [12], another NASA flight test experiment was made to reveal the forebody flow field of the receiver aircraft and two out of six capture attempts were successful. The capture criteria and miss criteria at the docking phase were also provided. The type of the tanker aircraft is Boeing 707-300 and the type of the receiver aircraft is F/A-18. The docking altitude and speed were both set to be constant. The actual flight test experiments were also conducted by North Atlantic Treaty Organization (NATO). In the ATP-56(B) issued by NATO [13], the tanker aircrafts are VC-10 and KC-10, and receiver aircraft is F-16A. The altitude range for refueling was from 1524 m to 6096 m and the speed range was from 118 m/s to 165 m/s. By facing different docking speeds and altitudes, a problem arises that what docking speed and altitude can make docking most easily. Motivated by this, this paper aims at studying the optimal speed and altitude based on the reachability analysis method. Concretely, different docking speeds and altitudes will correspond to different volumes of the reachable set at the docking phase, because they will change the relative motion model of the receiver aircraft with respect to the center of the drogue. Therefore, the speed and altitude corresponding to the maximum volume of reachable set are regarded as the optimal trim state.

It is reasonable to use the volume of the reachable set to measure how easy the docking is. The subset of the state space that can reach the target set while remaining in the acceptable range is called the reachable set [14]. With respect to the docking phase, the target set represents the set of successful docking states, and the reachable set is a set of the receiver aircraft states from which the docking maneuver can be accomplished within a finite time horizon. Thus, the larger the volume of the reachable set is, the higher probability the pilot or the UAV autopilot can drive the receiver aircraft to dock successfully. This further implies that it is more easily to dock. So far, the reachability analysis method has been applied to solve many problems, such as collision avoidance [14], control law design for safe aerobatic maneuvers [15], [16],

safety verification of autoland maneuvers [17] and a ground moving target tracking [18]. In [19], the reachability analysis method was first applied to an AR process. The AR process has been divided into several maneuver sequences and the reachability analysis method was used to design a maneuver decision to ensure safe operation of a sequential mode transition. Unlike [19], the aim of this paper is to determine the optimal trim state of the docking phase in terms of reachability.

The reachable set can be calculated by the Level Set Toolbox [20] based on the level set method [21]. Concretely, the computation of the optimal trim state for the considered docking phase of an AR process is divided into four phases. First, the trim state of the tanker aircraft is specified which is used in the relative motion model of the receiver aircraft with respect to the center of the drogue. Secondly, the state space is divided into grid points and the reachable set of the receiver aircraft is computed at each trim state. Thirdly, by comparing the volume of the reachable set at different trim states, the trim state of the tanker aircraft with the largest reachable set volume is regarded as the optimal trim state. Finally, the optimal trim state is verified by the docking control simulations and the degree of controllability from another aspect, showing that the docking success rate is the highest at the optimal altitude and speed. Therefore, the effectiveness of the proposed method is demonstrated. The contribution of this note is the idea and process of determining the optimal trim state for aerial docking for the first time.

2. Problem formulation

2.1. Relative motion model

Fig. 1 shows the docking phase of an AR process, where the origin of the system is at the center of the drogue of the tanker aircraft. The continuous-time dynamics between the tip of the probe and the center of the drogue in relative coordinates at the docking phase are considered at the docking phase. The state vector $\Delta \mathbf{x} = [\Delta V \ \Delta \gamma \ \Delta x \ \Delta h]^T$, whose elements represent the speed, flight path angle, longitudinal distance and altitude of the tip of the probe with respect to the center of the drogue, respectively. The longitudinal dynamics of the aircraft focused lie on two reasons: 1) it is more important than the lateral dynamics at the docking phase; 2) the objective is to determine the optimal trim state, for which longitudinal dynamics can simplify the problem without loss of generality.

The longitudinal dynamics of the receiver aircraft are modeled by using the reference frame shown in Fig. 2. The receiver aircraft is subject to the force of thrust T , lift L , drag D and gravity G . The state vector is $\mathbf{x}_r = [V_r \ \gamma_r \ x_r \ h_r]^T$, whose elements represent the speed, flight path angle, longitudinal distance and altitude of the mass center of the receiver aircraft, respectively. The control input is $\mathbf{u} = [T_r \ \alpha_r]^T$ whose elements denote the thrust and the angle of attack of the receiver aircraft, respectively. Therefore, the longitudinal dynamics of the mass center of the receiver aircraft are written as follows [17], [22]:

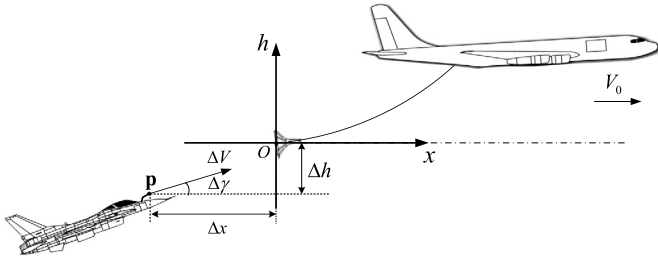


Fig. 1. Relative coordinate system of the docking phase of an AR process.

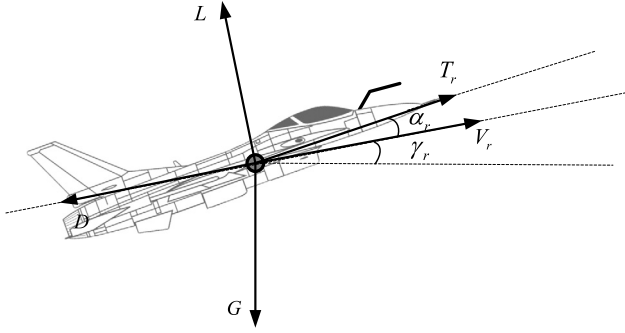


Fig. 2. Longitudinal dynamics of the receiver aircraft.

$$\begin{bmatrix} \dot{V}_r \\ \dot{\gamma}_r \\ \dot{x}_r \\ \dot{h}_r \end{bmatrix} = \begin{bmatrix} \frac{1}{m} (T_r \cos \alpha_r - D(\alpha_r, V_r) - mg \sin \gamma_r) \\ \frac{1}{mV_r} (T_r \sin \alpha_r + L(\alpha_r, V_r) - mg \cos \gamma_r) \\ V_r \cos \gamma_r \\ V_r \sin \gamma_r \end{bmatrix}. \quad (1)$$

The state vector of the tanker aircraft is $\mathbf{x}_t = [V_t \ \gamma_t \ x_t \ h_t]^T$, the elements of which represent the speed, the flight path angle, longitudinal distance and the altitude of the tanker aircraft, respectively. The state parameters V_t, h_t are assumed to be constant at the docking phase, namely

$$\dot{V}_t = 0, \dot{x}_t = V_t, \dot{h}_t = 0.$$

This implies $\gamma_t = 0$. To dock successfully, the receiver aircraft's speed should keep the same as the tanker aircraft. As a result, the trim state of the dynamic system Eq. (1) is $(V_0 \ \gamma_0 \ T_0 \ \alpha_0)$, where $V_0 = V_t, \gamma_0 = 0$. Based on the trim state and input, define

$$\Delta V_r = V_r - V_0, \Delta \gamma_r = \gamma_r - \gamma_0,$$

$$\Delta T_r = T_r - T_0, \Delta \alpha_r = \alpha_r - \alpha_0.$$

Then, Eq. (1) is rearranged to

$$\begin{bmatrix} \Delta \dot{V}_r \\ \Delta \dot{\gamma}_r \\ \Delta \dot{x}_r \\ \Delta \dot{h}_r \end{bmatrix} = \underbrace{\begin{bmatrix} \frac{1}{m} \left((T_0 + \Delta T_r) \cos(\alpha_0 + \Delta \alpha_r) - D(\alpha_0 + \Delta \alpha_r, V_0 + \Delta V_r) - mg \sin(\gamma_0 + \Delta \gamma_r) \right) \\ \frac{1}{m(V_0 + \Delta V_r)} \left((T_0 + \Delta T_r) \sin(\alpha_0 + \Delta \alpha_r) + L(\alpha_0 + \Delta \alpha_r, V_0 + \Delta V_r) - mg \cos(\gamma_0 + \Delta \gamma_r) \right) \\ (V_0 + \Delta V_r) \cos(\gamma_0 + \Delta \gamma_r) - V_0 \\ (V_0 + \Delta V_r) \sin(\gamma_0 + \Delta \gamma_r) \end{bmatrix}}_{\mathbf{f}_{h_0, V_0}(\Delta \mathbf{x}_r)}. \quad (2)$$

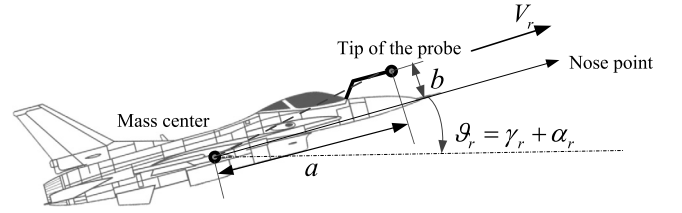


Fig. 3. Relative position of the tip of the probe with respect to the mass center of the receiver aircraft.

where the state vector $\Delta \mathbf{x}_r = [\Delta V_r \ \Delta \gamma_r \ \Delta x_r \ \Delta h_r]^T$ represents the speed, flight path angle, longitudinal distance and altitude of the mass center of the receiver aircraft with respect to the center of the drogue, respectively. Here, the lift and drag are expressed as [23]

$$\begin{aligned} L &= \frac{1}{2} \rho (V_0 + \Delta V_r)^2 C_L S \\ D &= \frac{1}{2} \rho (V_0 + \Delta V_r)^2 C_D S \end{aligned} \quad (3)$$

where ρ is the air density which is determined by the altitude of the tanker aircraft h_0 at the docking phase and S represents the wing area of the receiver aircraft. The lift coefficient C_L is a linear function of α_r given by

$$C_L = C_{L_0} + C_{L_\alpha}(\alpha_0 + \Delta \alpha_r), \quad (4)$$

where C_{L_0} is the lift coefficient at zero angle of attack and C_{L_α} is the lift coefficient slope. The drag coefficient C_D is computed by the following equation

$$C_D = C_{D_0} + K C_L^2, \quad (5)$$

where C_{D_0} is the zero lift drag coefficient which accounts for the drag of the body, the slats, the flags and the landing gear. The constant K is the lift-induced drag coefficient. According to Eqs. (3), (4), (5), the lift and drag depend on the parameters V_0 and h_0 . It implies that the speed and altitude of the tanker aircraft affect the lift and drag of the receiver aircraft, and further determine the dynamic model represented by Eq. (2).

2.2. Assumptions and objective

The relative position between the tip of the probe and the mass center of the receiver aircraft is presented in Fig. 3. As shown, ϑ_r is the angle of pitch, a and b represent the relative longitudinal distance and the relative altitude of the tip of the probe with respect to the mass center of the receiver aircraft. The relative position between the tip of the probe and the center of the drogue is

$$\begin{aligned} \Delta x &= \Delta x_r + (a \cos \vartheta_r - b \sin \vartheta_r) \\ \Delta h &= \Delta h_r + (a \sin \vartheta_r + b \cos \vartheta_r) \end{aligned} \quad (6)$$

The following assumptions are further made.

Assumption 1. At the docking phase, the control inputs of the receiver aircraft are limited by

$$\begin{aligned} \Delta T_{\min} &\leq \Delta T_r \leq \Delta T_{\max} \\ \Delta \alpha_{\min} &\leq \Delta \alpha_r \leq \Delta \alpha_{\max} \end{aligned} \quad (7)$$

Assumption 2. The speed and the flight path angle of the tip of the probe are equal to those of the receiver aircraft, given by

$$\begin{aligned} \Delta V &= \Delta V_r \\ \Delta \gamma &= \Delta \gamma_r \end{aligned} \quad (8)$$

Remark 1. The pilot of the manned aircraft or the UAV autopilot cannot change the control inputs aggressively during the docking phase. Thus, Assumption 1 is reasonable. At the docking phase, the pitch rate is small. Consequently, its effect on the speed and the flight path angle of the probe is ignored. Thus, Assumption 2 is also reasonable.

According to Eqs. (6)–(8), the relative motion between the center of the drogue and the tip of the probe is expressed as

$$\Delta \mathbf{x} = \mathbf{g}(\Delta \mathbf{x}_r). \quad (9)$$

Based on the Assumptions 1–2, the objective of this paper is to study the optimal trim state, including the optimal altitude and speed of the tanker aircraft at the docking phase by using the reachability analysis method. The optimal altitude and speed will be used to determine the trim state of the dynamic model described by Eq. (2). The docking speed and altitude of the tanker aircraft corresponding to the maximum volume of the reachable set is regarded as the optimal speed and altitude at the docking phase.

3. Computing procedure of the optimal trim state

For the docking phase of the AR process, the target set represents the state set of docking successfully and the reachable set is the state set of the receiver aircraft from which the docking phase can be completed within a finite time horizon $t \in [-\tau, 0]$. The target set \mathcal{D} and the reachable set $pre_\tau(\mathcal{D})$ can be regarded as the zero level set of the cost function $J(\mathbf{x}, t)$ at $t = 0$ and $t = -\tau$, respectively. The reachable set $pre_\tau(\mathcal{D})$ is computed by solving the following Hamilton-Jacobi Partial Differential Equation (HJ) PDE [14]

$$\begin{aligned} D_t J(\mathbf{x}, t) &= -H(\mathbf{x}, D_{\mathbf{x}} J(\mathbf{x}, t)) \\ \mathbf{x} &\in \mathcal{X}, t < 0 \\ J(\mathbf{x}, 0) &= J_0(\mathbf{x}), t = 0 \end{aligned} \quad (10)$$

backward from $t = 0$ until $H(\mathbf{x}, D_{\mathbf{x}} J(\mathbf{x}, t)) \approx 0$ or $t = -\tau$ and $D_t J(\mathbf{x}, t)$ represents the derivative of the cost function $J(\mathbf{x}, t)$. All the states of the target set \mathcal{D} and the reachable set $pre_\tau(\mathcal{D})$ are restricted by the state constraint set \mathcal{X} .

For the problem considered in this paper, the target set with respect to $\Delta \mathbf{x}$ showing in Fig. 1 can be expressed as

$$\mathcal{D}_{\Delta \mathbf{x}} = \{\Delta \mathbf{x} \in \mathbb{R}^4 | J(\Delta \mathbf{x}, 0) \leq 0\}. \quad (11)$$

Based on Eq. (9), the target set with respect to $\Delta \mathbf{x}_r$ can be written as

$$\mathcal{D}_{\Delta \mathbf{x}_r} = \{\Delta \mathbf{x}_r \in \mathbb{R}^4 | J(\mathbf{g}(\Delta \mathbf{x}_r), 0) \leq 0\}. \quad (12)$$

Through Eq. (12), the target set has been transformed into the range of states $\Delta \mathbf{x}_r$. Thus, the dynamic model $\Delta \dot{\mathbf{x}}_r = \mathbf{f}_{h_0, V_0}(\Delta \mathbf{x}_r)$ described in Eq. (2) is adopted to compute the volume of the reachable set.

Given altitude and speed (h_0, V_0) of the tanker aircraft at the docking phase, the cost function $J(\mathbf{x}, t)$ is rewritten as

$$J(\Delta \mathbf{x}_r, t, h_0, V_0) = J(\Delta \mathbf{x}_r, t)|_{h_0, V_0}. \quad (13)$$

The reachable set is denoted as

$$\Phi(h_0, V_0) = \{\Delta \mathbf{x}_r \in \mathcal{X}_r | J(\Delta \mathbf{x}_r, t, h_0, V_0) \leq 0, -\tau \leq t \leq 0\}, \quad (14)$$

where \mathcal{X}_r represents the state constraint set of the docking phase.

The volume of the reachable set with respect to (h_0, V_0) is defined by

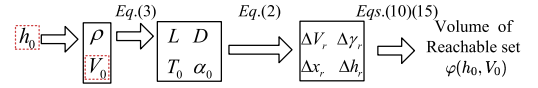


Fig. 4. Relationship between the docking speed V_0 docking altitude h_0 and the volume of reachable set $\varphi(h_0, V_0)$.

$$\varphi(h_0, V_0) = |\Phi(h_0, V_0)|, \quad (15)$$

where $|\cdot|$ represents the volume of the reachable set. The relationship between the trim state (h_0, V_0) of the tanker aircraft and the volume of the reachable set is shown in Fig. 4. The docking speed V_0 and altitude h_0 affect the volume of the reachable set through determining the trim state of Eq. (2).

The objective of this paper is to obtain the optimal trim state of the tanker aircraft at the docking phase. The optimal problem is transformed to find the optimal altitude and speed of the tanker aircraft to maximize the corresponding volume of the reachable set. The optimization problem is formulated as

$$\max_{h_0 \in [h_{\min}, h_{\max}], V_0 \in [V_{\min}, V_{\max}]} \varphi(h_0, V_0), \quad (16)$$

where $\varphi(h_0, V_0)$ is defined in Eq. (15). In the computing procedure, the reachable set is calculated on each grid of the continuous state space \mathcal{X}_r . The value $J(\Delta \mathbf{x}_r, t, h_0, V_0)$ of each grid of the reachable set is negative, thus the volume of the reachable set is measured by the number of negative grids in the state space \mathcal{X}_r . Thus, the optimal target is rewritten as

$$\max_{h_0 \in [h_{\min}, h_{\max}], V_0 \in [V_{\min}, V_{\max}]} \bar{\varphi}(h_0, V_0), \quad (17)$$

where $\bar{\varphi}(h_0, V_0)$ is a function representing the number of negative grids. The optimal solution to Eq. (17) can be seen as the approximate solution of Eq. (16), namely

$$\begin{aligned} (h_{op}, V_{op}) &= \arg \max_{h_0 \in [h_{\min}, h_{\max}], V_0 \in [V_{\min}, V_{\max}]} \varphi(h_0, V_0) \\ &\approx \arg \max_{h_0 \in [h_{\min}, h_{\max}], V_0 \in [V_{\min}, V_{\max}]} \bar{\varphi}(h_0, V_0). \end{aligned} \quad (18)$$

The simulation time step is set to $\Delta t = 0.1s$ and the backward computation time is $t = -i \times \Delta t$, $i = 1, 2, \dots, 10$. The computing procedure of the optimal trim state of the tanker aircraft is presented as follows:

Step 1. Initialize the state space, target set and the corresponding grid points.

Step 2. For the specified docking altitude h_0 and docking speed V_0 , calculate T_0 and α_0 .

Step 3. Repeat

Solve the HJ PDE (10) at each backward computation time $t = -i \times \Delta t$ to get the reachable set

until $t = -1s$ or $H(\mathbf{x}, D_{\mathbf{x}} J(\mathbf{x}, t)) \approx 0$.

Step 4. Calculate the volume of the reachable set for the selected docking altitude h_0 and docking speed V_0 according to $\bar{\varphi}(h_0, V_0)$.

Step 5. Obtain the optimal docking altitude h_{op} and speed V_{op} which correspond to the maximum volume of the reachable set.

4. Simulation analysis on the optimal docking altitude and speed of F-16 aircraft

4.1. Simulation description

A simplified nonlinear F-16 aircraft model is used to compute the optimal trim state based on the computing procedure proposed in Section 3. In this section, the system parameters of Eq. (2), the control constraint set, the state constraint set, the target set at the docking phase are provided.

Table 2
Physical parameters of F-16 aircraft model.

Parameters	m	g	S
Value	20500 lbs	9.8 m/s ²	300 ft ²

Table 3
Related parameters of dynamic model.

Parameters	C_{L_0}	C_{L_α}	C_{D_0}	K	a	b
Value	0.1	0.06	-0.021	0.35	3 m	0.5 m

Table 4
Limits of the variations of the control inputs of the dynamic model.

Variations of the control inputs	Min	Max
ΔT_r	-2000N	2000N
$\Delta \alpha_r$	-2°	2°

(i) **System Parameters.** The physical parameters of the F-16 aircraft model are shown in Table 2. The related parameters used in Eq. (2) are given in Table 3. The lift coefficient C_L and drag coefficient C_D are obtained through the linear interpolation in the lift curve and drag curve of the F-16 aircraft [17].

(ii) **Control Constraint Set.** As presented in Section 2, $T_r = T_0 + \Delta T_r$ and $\alpha_r = \alpha_0 + \Delta \alpha_r$. As shown in Fig. 4, T_0 and α_0 are determined by the trim state (h_0, V_0) of the tanker aircraft. The limits of the control inputs of the Eq. (2) are provided in Table 4.

(iii) **State Constraint Set.** The Cartesian grid is used to approximate the state space \mathcal{X}_r . The ranges of the states of the system and the grid division are shown in Table 5. If the states are out of the ranges, then the docking is considered to fail. The grid division needs to satisfy the Courant-Friedrichs-Lewy (CFL) condition to ensure the stability of the computing results [20].

(iv) **Target Set.** A neighborhood around the desired final states at the docking phase is chosen as the target set. For the considered system, the target set with respect to $\Delta \mathbf{x}$ is

$$\mathcal{D}_X = \left\{ \Delta \mathbf{x} \in \mathbb{R}^4 \mid J(\Delta \mathbf{x}, 0) = \max \begin{pmatrix} \max(\Delta \tilde{V} - \Delta V_{up}, \Delta V_{low} - \Delta \tilde{V}), \\ \max(\Delta \tilde{\gamma} - \Delta \gamma_{up}, \Delta \gamma_{low} - \Delta \tilde{\gamma}), \\ \max(\Delta \tilde{x} - \Delta x_{up}, \Delta x_{low} - \Delta \tilde{x}), \\ \max(\Delta \tilde{h} - \Delta h_{up}, \Delta h_{low} - \Delta \tilde{h}) \end{pmatrix} \leq 0 \right\}, \quad (19)$$

where $\Delta \tilde{\mathbf{x}} = [\Delta \tilde{V} \ \Delta \tilde{\gamma} \ \Delta \tilde{x} \ \Delta \tilde{h}]^T$ represents the state vector of each grid point and $\Delta V_{up} = 2 \text{ m/s}$, $\Delta V_{low} = -0.2 \text{ m/s}$, $\Delta \gamma_{up} = 0.5^\circ$, $\Delta \gamma_{low} = -0.5^\circ$, $\Delta x_{up} = 0 \text{ m}$, $\Delta x_{low} = -0.3 \text{ m}$, $\Delta h_{up} = 1 \text{ m}$, $\Delta h_{low} = -1 \text{ m}$ which represent the upper and lower boundary of the target set. Based on Eq. (19), the target set can be rewritten as

$$\mathcal{D}_X = \left\{ \Delta \mathbf{x} \in \mathbb{R}^4 \mid \begin{matrix} -0.2 \text{ m/s} \leq \Delta V \leq 2 \text{ m/s}, \\ -0.5^\circ \leq \Delta \gamma \leq 0.5^\circ, \\ -0.3 \text{ m} \leq \Delta x \leq 0 \text{ m}, \\ -1 \text{ m} \leq \Delta h \leq 1 \text{ m} \end{matrix} \right\}. \quad (20)$$

At the docking phase γ_t and γ_r approach zero degree, namely $\gamma_t = \gamma_r \approx 0^\circ$. Thus, in Fig. 3, $\vartheta_r \approx \alpha_r$. The parameter α_r is small at the docking phase leading to $\vartheta_r \approx 0^\circ$. Through the transformation of Eq. (12), the target set specified in the relative coordinate system is expressed by

Table 5
Grid division of the state space.

Parameters	$\Delta V_r \text{ (m/s)}$	$\Delta \gamma_r \text{ (deg)}$	$\Delta x_r \text{ (m)}$	$\Delta h_r \text{ (m)}$
Range	[-2, 7]	[-10, 5]	[-4, 0.5]	[-1, 1]
Grid numbers	40	30	20	20
Step size	0.23	0.5	0.23	0.1

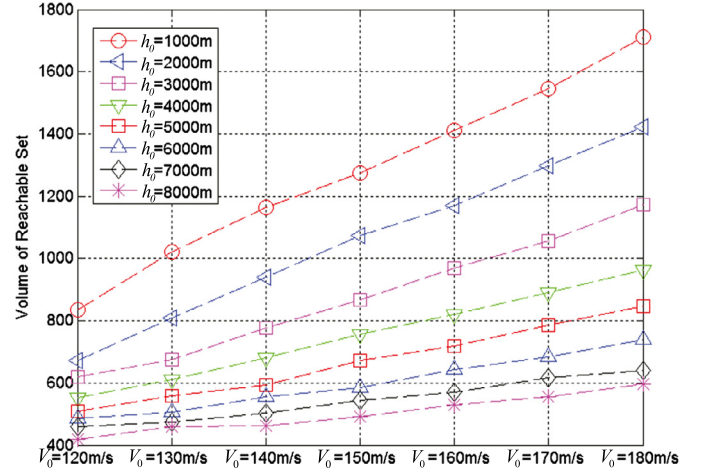


Fig. 5. Volume of reachable set at different altitudes and different docking speeds.

$$\mathcal{D}_{X_r} = \left\{ \Delta \mathbf{x}_r \in \mathbb{R}^4 \mid \begin{matrix} -0.2 \text{ m/s} \leq \Delta V_r \leq 2 \text{ m/s}, \\ -0.5^\circ \leq \Delta \gamma_r \leq 0.5^\circ, \\ (-0.3 - a) \text{ m} \leq \Delta x_r \leq (-a) \text{ m}, \\ (-1 - b) \text{ m} \leq \Delta h_r \leq (1 - b) \text{ m} \end{matrix} \right\}, \quad (21)$$

where the target set \mathcal{D}_{X_r} is a small hypercube.

Remark 2. The target set is a four-dimensional (4D) hypercube. So, the function $J(\Delta \mathbf{x}, 0)$ in Eq. (19) is not differentiable. However, the HJ PDE can be still solved by a numerical method. According to Eq. (19), the distance between each grid point and the boundary of the target set can be obtained by the function "ShapeRectangleByCorners" in the ToolboxLS [20]. For the discrete grid points, the derivative of $J(\Delta \mathbf{x}_r, t)|_{h_0, V_0}$ can be computed.

Remark 3. The primary weakness of the reachability analysis method is that memory and computational time requirements rise exponentially with dimension. In practice, systems of dimensions 1~3 can be examined interactively [14]. The dimension of the longitudinal dynamics of the mass center of the receiver aircraft is four. It is slow but feasible on a computer with sufficient memory. Since the exact computation of reachable set is typically done off-line, the over-approximating reachable set can allow for real-time computation [15].

4.2. Optimal docking speed and docking altitude

In this section, the volumes of the reachable set at different docking altitudes and speeds are depicted in Fig. 5. The computation of reachable set is typically done off-line in Matlab, and run on a desktop with 2.4 GHz CPU and 2 GB RAM. The computation time is 986.878 seconds at each discrete altitude and speed. Furthermore, the computation time of the volumes of the reachable set is 0.000046 s. The Matlab source code of the paper is presented in our research group website <http://rfly.buaa.edu.cn/resources/>. The altitude and speed of the F-16 aircraft at the docking phase is confined to 1000 m ~ 8000 m with the interval 1000 m and 120 m/s ~ 180 m/s with the interval 10 m/s, respectively. The volume of the reachable set at discrete altitude and speed is

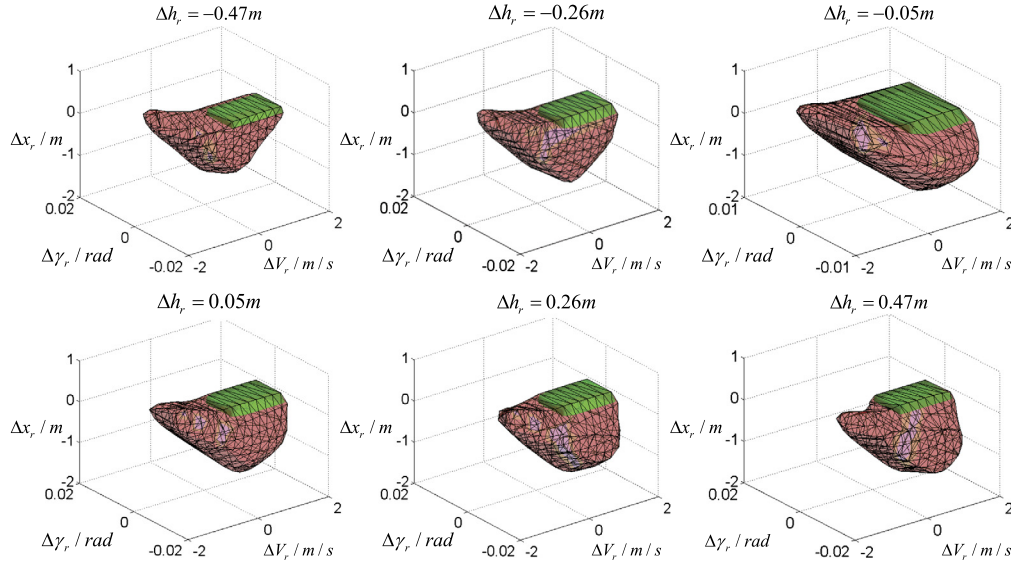


Fig. 6. Target set (green) and reachable set (red) for three-dimensional (3D) slices of the four-dimensional (4D) reachable set with the optimal altitude $h_{op} = 1000$ m and the optimal docking speed $V_{op} = 180$ m/s. (For interpretation of the colors in the figure(s), the reader is referred to the web version of this article.)

$$\begin{aligned}
 RS_{ij} &= \bar{\varphi}(h(i), V(j)) \\
 h(i) &= 1000 + 1000 * i, \quad i = 0, 1, 2, \dots, 7. \\
 V(j) &= 120 + 10 * j, \quad j = 0, 1, 2, \dots, 6
 \end{aligned} \quad (22)$$

From the obtained results in Fig. 5, three observations can be concluded. (i) As the altitude changes from 1000 m to 8000 m, the volume of the reachable set $\bar{\varphi}(h_0, V_0)$ is monotonously decreased. (ii) The volume of the reachable set $\bar{\varphi}(h_0, V_0)$ at a high altitude is always small regardless of the docking speed. (iii) As the speed changes from 120 m/s to 180 m/s, the volume of the reachable set $\bar{\varphi}(h_0, V_0)$ is monotonously increased. This implies that the faster the tanker aircraft is, the bigger state space the receiver aircraft can be operated in. Then, the optimal docking altitude h_{op} and optimal speed V_{op} are obtained by

$$(h_{op}, V_{op}) = \arg \max_{h_0 \in [h_{\min}, h_{\max}] V_0 \in [V_{\min}, V_{\max}]} \bar{\varphi}(h_0, V_0). \quad (23)$$

They are $h_{op} = 1000$ m and $V_{op} = 180$ m/s. The corresponding maximum volume of the reachable set is $\bar{\varphi}(h_{op}, V_{op}) = 1710$.

The reasons for these observations are summarized as follows. (i) As the altitude is increased, the air density is decreased. Therefore, the receiver aircraft should increase the speed to balance the gravity and the drag force. Meanwhile, the maneuverability of the aircraft becomes worse at a high altitude, resulting in a small volume of the reachable set. (ii) The air density is increased as the altitude is decreased, and the maneuverability of the aircraft becomes better. Thus, the corresponding volume of the reachable set is bigger. This implies that it is suitable for docking at a low altitude. However, by considering the air turbulence and the operational risk of the pilots, it is better to dock at a medium altitude and a medium speed for safety considerations.

The further explanation is provided as follows. The maneuverability is roughly related to the feasible control input of an aircraft. The larger the maneuverability, the more margin the feasible control can offer, implying a larger reachability roughly [24]. Compared with the maneuverability, the proposed reachability is more exact as it has taken both control input and the system dynamics into consideration. Often, the maneuverability of an aircraft is measured by the normal load factor n_y which can be expressed as $n_y = L/G$. The gravity G is constant. If the lift L is larger, its corresponding normal load n_y is larger, i.e., the maneuverability is better. According to the Fig. 5, two cases are considered. In the first

case, the speed V is set to be constant and the altitude h_1 is set to be higher than the altitude h_2 which are both between 1000 m and 8000 m. The air densities at the altitudes h_1 and h_2 are supposed to be ρ_1 and ρ_2 , respectively. The formula of the Mach number is $M = V/V_a$, where V_a represents the speed of sound. The Mach number at the altitude h_1 and h_2 are set to be M_1 and M_2 , respectively. According to the formula of the lift L which has been provided in Eq. (3), the lift at the altitude h_1 and h_2 can be expressed as $L_1 = \frac{1}{2} \rho_1 V^2 C_{L1} S$ and $L_2 = \frac{1}{2} \rho_2 V^2 C_{L2} S$. As the altitude is increased, the air density ρ is decreased, namely $\rho_1 < \rho_2$. Meanwhile, the speed of sound V_a is also decreased, implying the Mach number $M_1 > M_2$ and the corresponding lift coefficient $C_{L1} < C_{L2}$. Thus, the lift L_2 is larger than the lift L_1 and then the maneuverability at the altitude h_2 is better. This means that if the aircraft speed V is constant, then the volumes of the reachable set at altitude h_2 is larger because the maneuverability at the altitude h_2 is better. In the second case, the altitude h is set to be constant and the speed V_1 is set to be larger than the speed V_2 which are both between 120 m/s and 180 m/s. According to the definition of the lift L , the lifts at the speed V_1 and the speed V_2 can be expressed as $L_1 = \frac{1}{2} \rho V_1^2 C_L S$ and $L_2 = \frac{1}{2} \rho V_2^2 C_L S$, respectively. It is obvious that the lift L_1 is larger than L_2 . This implies that the maneuverability at the speed V_1 is better than that at the speed V_2 . Therefore, if the aircraft altitude h is set to be constant, then the volume of the reachable set at speed V_1 is larger than that at the speed V_2 .

The Fig. 6 shows the 3D slices of the 4D maximum reachable set. The 4D maximal reachable set is the largest controllable set from which the receiver aircraft can dock successfully.

4.3. Verification

4.3.1. Verification by using LQR controllers

In this section, LQR controllers are used to verify the optimal trim state at the docking phase. It is reasonable to adopt LQR controller to verify the simulation results owing the fact that LQR approach is often employed to design the docking control laws for the AR process [3], [25], [26]. The number of docking success grids of the reachable set at different altitudes and speeds within a specified time horizon is used to measure how difficult the docking is. If the number is larger, it means that it is easier to dock with the

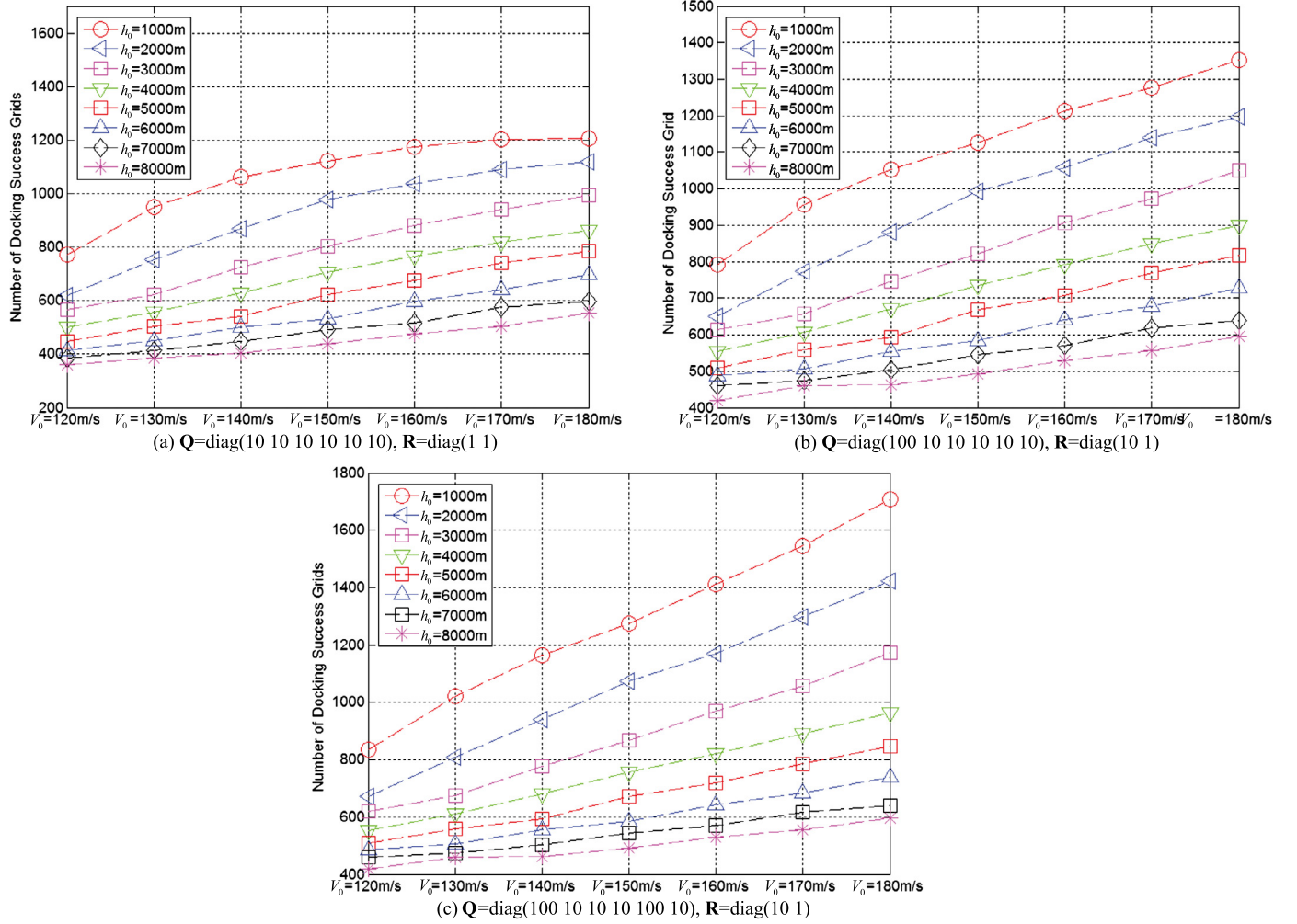


Fig. 7. For different matrix \mathbf{Q} and \mathbf{R} , the numbers of docking success grid at different altitudes and speeds.

corresponding controller. The main steps of verification are shown as follows:

Step 1. Calculate T_0 and α_0 at the docking altitude h_0 and docking speed V_0 .

Step 2. Linearize the dynamic model of the system as in Eq. (2) which is written as

$$\Delta \dot{\mathbf{x}}_r = \mathbf{A}_r \Delta \mathbf{x}_r + \mathbf{B}_r \mathbf{u},$$

where

$$\mathbf{A}_r = \begin{bmatrix} -\frac{\rho V_0 S C_d}{m} & -g \cos \gamma_0 & 0 & 0 \\ \frac{\frac{1}{2} \rho V_0^2 S C_L - T_0 \sin \alpha_0 + mg \cos \gamma_0}{m V_0^2} & \frac{g \sin \gamma_0}{V} & 0 & 0 \\ \cos \gamma_0 & -V_0 \sin \gamma_0 & 0 & 0 \\ \sin \gamma_0 & V_0 \cos \gamma_0 & 0 & 0 \end{bmatrix},$$

$$\mathbf{B}_r = \begin{bmatrix} -\frac{T_0 \sin \alpha_0}{m} & \frac{\cos \alpha_0}{m} \\ -\frac{T_0 \cos \alpha_0}{m V_0} & \frac{\sin \alpha_0}{m V_0} \\ 0 & 0 \\ 0 & 0 \end{bmatrix}.$$

Step 3. Each grid point of the reachable set at the selected docking altitude h_0 and docking speed V_0 is taken as the initial state of the LQR controllers (see the Appendix A for details). The controllers are used to drive the state of the receiver aircraft into the target set \mathcal{D} . The control time is set to be 5 s, which is longer than the backward computation time of the reachable set. This is because the LQR controllers need enough time to converge.

Step 4. Record the number of docking success grid of the reachable set which can be defined as $\tilde{\varphi}(h_i, V_j)$ at different altitudes and speeds.

The numbers of docking success grid for three LQR controllers are depicted in Fig. 7. As shown, two observations can be concluded. (i) The $\tilde{\varphi}(h_i, V_j)$ is proportional with $\tilde{\varphi}(h_i, V_j)$. (ii) The maximum number of the docking success grid for different LQR controllers are 1207, 1353 and 1708 with altitude $h_i = 1000$ m and docking speed $V_j = 180$ m/s which corresponds with the maximum volume of the reachable set. The verification of the results leads to the following conclusions. (i) The success rate of the LQR controller is proportional with the volume of reachable set. (ii) It is more suitable to design controllers at the optimal trim state at the docking phase.

4.3.2. Verification by using degree of controllability

In this section, a degree of controllability (DoC) is adopted to verify the effectiveness of the proposed method from another aspect. The linear dynamical model of the system is $\Delta \dot{\mathbf{x}}_r = \mathbf{A}_r \Delta \mathbf{x}_r + \mathbf{B}_r \mathbf{u}$, where the control input $\mathbf{u} = [T_r \ \alpha_r]^T \in \Omega$. The definitions of recovery region and DoC are obtained according to [27].

Definition 1. For the linear dynamical model of the system, the recovery region \mathcal{R} within time t_r is defined as

$$\mathcal{R}(t_r) = \{ \Delta \mathbf{x}_r(0) \mid \exists \mathbf{u}(t) \in \Omega, t \in [0, t_r], \text{ s.t. } \Delta \mathbf{x}_r(t_r) = \mathbf{0} \} \quad (24)$$

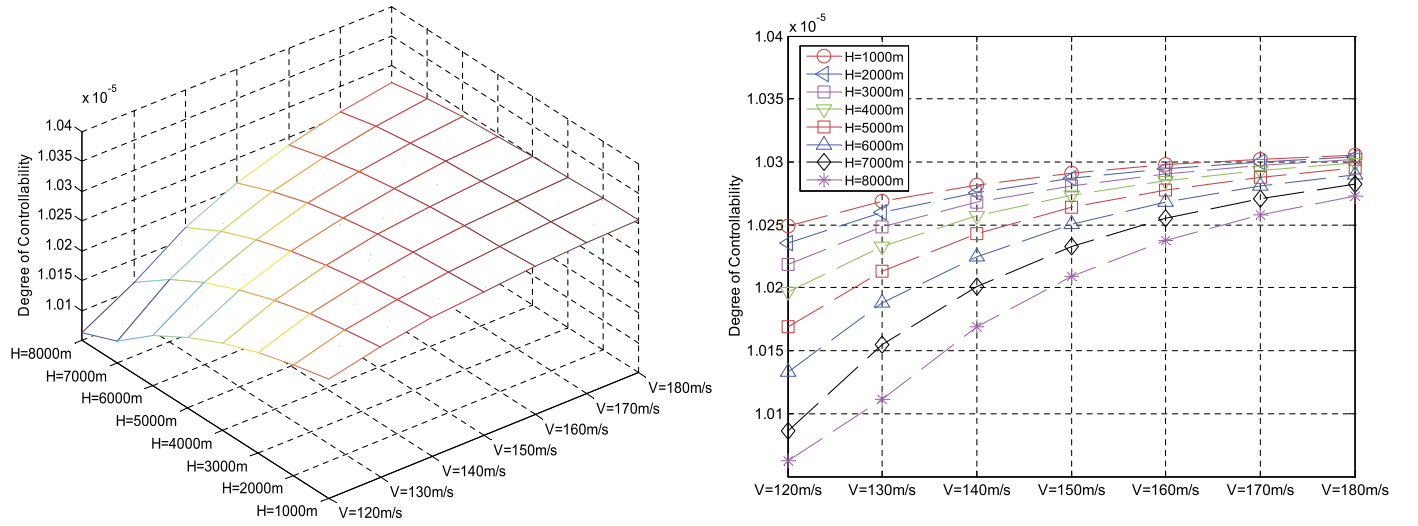


Fig. 8. (Left) Three-dimensional surface and (right) two-dimensional curve of the value of ρ_{doc} at different altitudes and speeds.

Definition 2. For the linear dynamical model of the system, the DoC ρ within time t_r is defined as

$$\rho_{doc} = \inf \|\Delta \mathbf{x}_r(0)\| \quad \forall \Delta \mathbf{x}_r(0) \notin \mathcal{R}(t_r) \quad (25)$$

where $\|\cdot\|$ represents the Euclidean norm.

From Definition 2, it is observed that the minimal distance from the origin to the boundary of the recovery region is considered to be the DoC of the system. The value of ρ_{doc} represents how controllable the system is. The larger the value of ρ_{doc} , the stronger the system control ability is. The values of ρ_{doc} at different altitudes and speeds can be defined as $\rho_{doc}(h_i, V_j)$ which are shown in Fig. 8. As shown in Fig. 8, the $\rho_{doc}(h_i, V_j)$ is proportional with $\bar{\varphi}(h_i, V_j)$. This shows the feasibility of our simulation results from another aspect. The use of DoC is not used to replace with the reachability analysis but is only taken as a verification for the reachability analysis, because i) the target set is only zero rather than a set as in Eq. (12) for reachability analysis here; ii) a linear model is used rather than nonlinear model used for the reachability analysis.

5. Conclusions

In order to improve the success rate of docking in an AR process, the reachability analysis method is used to obtain the optimal trim state of the tanker aircraft at the docking phase. The optimal trim state is defined as the docking state of the tanker aircraft corresponding to the maximum volume of the reachable set. First, in order to find the optimal trim state of the tanker aircraft at the docking phase, 4D relative motion model between the receiver aircraft and the center of the drogue is proposed. Based on it, a step-by-step computing procedure to obtain the optimal docking speed and altitude is proposed. Then, the simulation on a simplified nonlinear F-16 aircraft model is studied comprehensively. From the simulation, the success rate of the proposed LQR controller is proportional with the volume of the reachable set so that the proposed method to obtain the optimal trim state of the tanker aircraft is reasonable. Furthermore, a DoC method is also used to verify the feasibility of the optimal trim state from another aspect.

For the simulation results, the brute force search method is used to determine the optimal trim state. From the simulation results obtained, the problem seems like convex optimization problem. But it is difficult to verify the convexity of the simulation results, the major reason for which is the function of the volume

of the reachable set is not easy to use an analytical function to express. But the convexity of the simulation results is also a problem which is needed to be solved. The verification of its convexity of the optimization problem is regarded as the further study.

Declaration of competing interest

The authors have no affiliation with any organization with a direct or indirect financial interest in the subject matter discussed in the manuscript.

Acknowledgements

This work was supported by the National Natural Science Foundation of China under Grant 61473012.

Appendix A

The LQR controller is used to drive the state of each grid into the target set \mathcal{D}_r . The design process is summarized as follows. First, introduce an integral term $\Delta \dot{\mathbf{x}}_r' = -f \mathbf{C}^T \Delta \mathbf{x}_r$, where

$$\mathbf{C} = \begin{bmatrix} 0 & 0 & 1 & 0 \\ 0 & 0 & 0 & 1 \end{bmatrix}.$$

Let $\Delta \mathbf{x}_r^a = [\Delta \mathbf{x}_r^T \quad \Delta \dot{\mathbf{x}}_r'^T]^T$. Then

$$\Delta \dot{\mathbf{x}}_r^a = \mathbf{A} \Delta \mathbf{x}_r^a + \mathbf{B} \mathbf{u} \quad (26)$$

where

$$\mathbf{A} = \begin{bmatrix} \mathbf{A}_r & \mathbf{0}_{4 \times 2} \\ -\mathbf{C} & \mathbf{0}_{2 \times 2} \end{bmatrix}, \mathbf{B} = \begin{bmatrix} \mathbf{B}_r \\ \mathbf{0}_{2 \times 2} \end{bmatrix}.$$

The LQR controller is designed based on Eq. (26), where the matrixes \mathbf{Q} and \mathbf{R} are given in three cases: (i) $\mathbf{Q} = \text{diag}(10, 10, 10, 10, 10, 10)$, $\mathbf{R} = \text{diag}(1, 1)$; (ii) $\mathbf{Q} = \text{diag}(100, 10, 10, 10, 10, 10)$, $\mathbf{R} = \text{diag}(10, 1)$; (iii) $\mathbf{Q} = \text{diag}(100, 10, 10, 10, 100, 10)$, $\mathbf{R} = \text{diag}(10, 1)$.

References

- [1] J.P. Nalepka, J.L. Hinchman, Automated aerial refueling: extending the effectiveness of unmanned air vehicles, in: AIAA Modeling and Simulation Technologies Conference and Exhibit, San Francisco, California, Aug. 2005, pp. 15–18.
- [2] P.R. Thomas, U. Bhandari, Advances in air to air refuelling, Prog. Aerosp. Sci. 14 (35) (2014) 14–35.

- [3] Y.H. Liu, H.L. Wang, Z.K. Su, et al., Deep learning based trajectory optimization for UAV aerial refueling docking under bow wave, *Aerosp. Sci. Technol.* 80 (2018) 392–402.
- [4] Y.H. Liu, H.L. Wang, J.X. Fan, et al., Novel docking controller for autonomous aerial refueling with probe direct control and learning-based preview method, *Aerosp. Sci. Technol.* 94 (2019) 1–14.
- [5] J.R. Ren, X.H. Dai, Q. Quan, et al., Reliable docking control scheme for probe-drogue refueling, *J. Guid. Control Dyn.* 42 (11) (2019) 2511–2520.
- [6] L.X. Wang, H.P. Yin, Y.G. Guo, et al., Closed-loop motion characteristic requirements of receiver aircraft for probe and drogue aerial refueling, *Aerosp. Sci. Technol.* 93 (2019) 1–10.
- [7] X.H. Dai, Z.B. Wei, Q. Quan, et al., Hose-drum-unit modeling and control for probe-and-drogue autonomous aerial refueling, *IEEE Trans. Aerosp. Electron. Syst.* 56 (4) (2020) 2779–2791.
- [8] X.H. Dai, Q. Quan, J.R. Ren, et al., Iterative learning control and initial value estimation for probe-drogue autonomous aerial refueling of UAVs, *Aerosp. Sci. Technol.* 82–83 (2018) 583–593.
- [9] Z.B. Wei, X.H. Dai, Q. Quan, et al., Drogue dynamic model under bow wave in probe-and-drogue refueling, *IEEE Trans. Aerosp. Electron. Syst.* 52 (4) (2016) 1728–1742.
- [10] H.T. Wang, X.M. Dong, J.P. Xue, et al., Dynamic modeling of a hose-drogue aerial refueling system and integral sliding mode backstepping control for the hose whipping phenomenon, *Chin. J. Aeronaut.* 29 (2) (2016) 335–345.
- [11] J.H. Hensen, J.E. Murray, N.V. Campos, The NASA Dryden AAR project: a flight test approach to an aerial refueling system, in: *AIAA Atmospheric Flight Mechanics Conference & Exhibit*, Aug. 2004, pp. 2004–4939.
- [12] R. Dibley, M. Allen, N. Nabaa, Autonomous airborne refueling demonstration phase I flight-test results, in: *AIAA Atmospheric Flight Mechanics Conference and Exhibit*, Aug. 2007, pp. 20–23.
- [13] NATO, ATP-56(B) air-to-air refuelling, Tech. Report, NATO, 2010.
- [14] I.M. Mitchell, A.M. Bayen, C.J. Tomlin, A time-dependent Hamilton-Jacobi formulation of reachable sets for continuous dynamic games, *IEEE Trans. Autom. Control* 50 (7) (2005) 947–957.
- [15] J.H. Gillula, G.M. Hoffmann, Applications of hybrid reachability analysis to robotic aerial vehicles, *Int. J. Robot. Res.* 30 (3) (2011) 335–354.
- [16] T. Lombaerts, S.R. Schuet, K.R. Wheeler, Safe maneuvering envelope estimation based on a physical approach, in: *AIAA Guidance, Navigation, and Control (GNC) Conference*, Boston, Aug. 2013, pp. 1–20.
- [17] A.M. Bayen, I.M. Mitchell, Aircraft autolander safety analysis through optimal control based reachable set computation, *J. Guid. Control Dyn.* 30 (1) (2007) 68–77.
- [18] J.H. Gillulay, C.J. Tomlin, Guaranteed safe online learning of a bounded system, in: *Intelligent Robots and Systems, IEEE/RSJ International Conference*, San Francisco, Sep. 2011, pp. 2979–2984.
- [19] J. Ding, J. Sprinkle, C.J. Tomlin, Reachability calculations for vehicle safety during manned/unmanned vehicle interaction, *J. Guid. Control Dyn.* 35 (1) (2012) 138–152.
- [20] I.M. Mitchell, A toolbox of level set methods, Tech. Rep. TR-2004-09, Dept. Comput. Sci., Univ. British Columbia, Vancouver, BC, Canada, 2004, pp. 99–114, <http://www.cs.ubc.ca/~mitchell/ToolboxLS/toolboxLS.pdf>.
- [21] S. Osher, *Level Set Methods and Dynamic Implicit Surfaces*, Springer, 2003, pp. 25–37.
- [22] F. Gavilan, R. Vazquez, J. Acosta, Adaptive control for aircraft longitudinal dynamics with thrust saturation, *J. Guid. Control Dyn.* 38 (4) (2014) 651–661.
- [23] B.L. Stevens, *Aircraft Control and Simulation: Dynamics, Controls Design, and Autonomous Systems*, John Wiley & Sons, 2003, pp. 68–77.
- [24] M.G. Goman, A.V. Khrantsovsky, E.N. Kolesnikov, Evaluation of aircraft performance and maneuverability by computation of attainable equilibrium sets, *J. Guid. Control Dyn.* 31 (2) (2015) 329–339.
- [25] G. Campa, M.R. Napolitano, M.L. Fravolini, Simulation environment for machine vision based aerial refueling for UAVs, *IEEE Trans. Aerosp. Electron. Syst.* 71 (1) (2009) 138–151.
- [26] M.D. Tandale, R. Bowers, J. Valasek, Trajectory tracking controller for vision-based probe and drogue autonomous aerial refueling, *J. Guid. Control Dyn.* 29 (4) (2012) 846–857.
- [27] G.X. Du, Q. Quan, B.X. Yang, et al., Controllability analysis for multirotor helicopter rotor degradation and failure, *J. Guid. Control Dyn.* 38 (5) (2015) 978–985.